

RF and mm-wave photonics at Sandia National Laboratories

G. Allen Vawter and Charles Sullivan

Sandia National Laboratories
P.O. Box 5800, Albuquerque, NM 87185-0603

ABSTRACT

RF and mm-wave photonic devices and circuits have been developed at Sandia National Laboratories for applications ranging from RF optical data links to optical generation of mm-wave frequencies. This talk will explore recent high-speed photonics technology developments at Sandia including: 1) A monolithic optical integrated circuit for all-optical generation of mm-waves. Using integrated mode-locked diode lasers, amplifiers, and detectors, frequencies between 30 GHz and 90 GHz are generated by a single monolithic (Al,Ga)As optical circuit less than 2mm in its largest dimension. 2) Development of polarization-maintaining, low-insertion-loss, low v-pi, Mach-Zehnder interferometer (MZI) modulators with DC-to-potentially-K-band modulation bandwidth. New low-loss polarization-maintaining waveguide designs using binary alloys have been shown to reduce polarization crosstalk in undoped (Al,Ga)As waveguides, yielding high extinction ratio (>40dB) and low on-chip loss (<6dB) in Mach-Zehnder interferometers. RF drive voltage is reduced through use of 45mm-active length devices with modulator sensitivity, v-pi, less than 3V.

Keywords: terahertz and gigahertz photonic components, integrated optics, mach-zehnder interferometer, diode laser, mode-locking, optical waveguide, AlGaAs, mm-wave, optoelectronic integrated circuit, OEIC, optical modulator

1. INTRODUCTION

Sandia National Laboratories has a wide variety of interests in RF and mm-wave photonic devices and circuits. This paper summarizes a few of the recent projects with emphasis on both new all-optical functionality and hard-won refinements making (Al,Ga)As photonic integrated circuits (PICs) viable in real-world systems applications. Three different devices will be discussed: 1) A monolithic optical integrated circuit using integrated mode-locked diode lasers, amplifiers, and detectors for all-optical generation of mm-waves.¹ 2) Development of polarization-maintaining, low-insertion-loss, low v-pi, Mach-Zehnder interferometer modulators with DC-to-potentially-K-band modulation bandwidth. New low-loss polarization-maintaining waveguide designs using binary alloys have been shown to reduce polarization crosstalk in undoped (Al,Ga)As waveguides, yielding high extinction ratio (>40dB) and low on-chip loss (<6dB) in Mach-Zehnder interferometers. 3) Adiabatic mode transforming tapered waveguides for extremely efficient coupling of light into and out of high-speed semiconductor optical waveguide circuits and devices.

2. PIC FOR ALL-OPTICAL MILLIMETER-WAVE SIGNAL GENERATION

Generation of mm-wave signals presently requires discrete negative differential resistance diodes coupled to a metallic waveguide cavity resonant at the desired frequency. At frequencies near 100 GHz, the output power and efficiency of these sources is low (typically 10 mW output power and $\leq 1\%$ efficiency); and higher frequencies are only accessible by frequency mixing. Demonstration of passive mode-locking of semiconductor ring lasers at high pulse repetition rates² suggests the possibility of a photonic

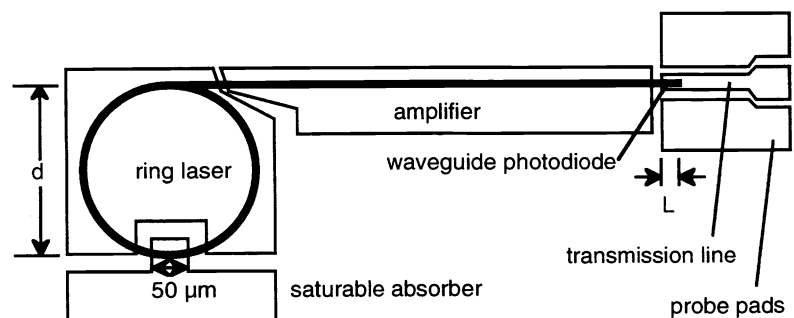


Figure 1: Schematic of actual mm-wave generation circuit.

integrated circuit comprising a mode-locked ring laser and traveling-wave photodiode³⁻⁵ (TWPD) for direct generation of mm-wave electrical signals. Such a PIC could be much more compact and efficient compared to current technology and

operate in the regime above 60 GHz where existing semiconductor-based mm-wave sources are inefficient or simply non-existent.

In this letter, we demonstrate the first monolithic PIC for generation of mm-wave signals. This new PIC integrates a passively mode-locked semiconductor ring laser, optical amplifier and high-speed photodiode for generation, amplification and detection of an optical pulse train with 30 to 90 GHz pulse-repetition frequency. Output is an electrical signal, generated by the photodiode, whose fundamental frequency is the pulse repetition rate of the mode-locked laser. The circuit uses a novel waveguide photodiode (WGPD) integrated with a mm-wave transmission line specifically designed for high-speed operation and signal extraction on a heavily-doped GaAs substrate.

The mm-wave signal generation PIC design for 60 and 90 GHz signals is shown in Fig. 1. A closed-ring GaAs/AlGaAs diode laser with a separately contacted, reverse-biased saturable absorber is passively mode locked generating a continuous train of short (1 to 10 ps) optical pulses in the ring cavity. Output of the ring laser is coupled to optical waveguide amplifier using a multi-mode Y-junction. A direct-waveguide photodetector (WGPD) converts the optical pulse train emerging from the amplifier to a mm-wave

electrical output. Finally, a 50-Ohm transmission line is integrated with the WGPD for removal of the electrical signal. A WGPD was chosen rather than a velocity-matched TWPD so that the PIC requires only one epitaxial growth sequence. The pn-junction design is optimized for laser and amplifier operation and does not have a large enough depletion width to accommodate a velocity-matched photodetector. An alternate configuration was used for 30 GHz signals wherein the reverse-biased saturable absorber also functions as a high-speed photodetector, converting a fraction the lasing pulse train into a mm-wave electrical output. Although more simple, this configuration does not offer the output power potential of the PIC using an optical amplifier and WGPD.

2.1 Design

The pulse repetition frequency, f , of the mode-locked laser is fixed by the cavity round trip time which is determined by the diameter of the ring according to (1)

$$f = \frac{c}{n_{\text{eff}}} \times \frac{1}{\pi d} \quad (1)$$

where c is the vacuum speed of light, n_{eff} the *group* effective refractive index of the multimode ring waveguide and d the ring diameter. Using the known 86 GHz rate for a 300 μm ring employing 6- μm wide multilateral-moded rib waveguides, rings of nominally 30, 60 and 90 GHz pulse-repetition frequency were designed having diameters of 860, 430 and 290 μm respectively. Light output from the ring laser is coupled by an equal-width branching Y-junction into a 1-mm long waveguide optical amplifier providing optical gain to the pulse train prior to coupling into the WGPD. Fig. 2 shows cross sections of the four circuit elements.

The WGPD was designed for high-speed operation and minimum capacitive loading caused by the n-type doped substrate. The WGPD, Fig. 2b, has a small active area and is coupled directly into a 50 Ohm transmission line, Fig. 2c, and ground-signal-ground contact pads. Dimensions of the transmission line were selected to give low loss and 50 Ohm characteristic impedance. The WGPD is fabricated by inserting the pn-junction waveguide material between the center electrode and ground plane of the transmission line. The additional loss and capacitance of the diode lowers the characteristic impedance and raises the effective refractive index sufficiently that device lengths below 200 μm are adequately viewed as

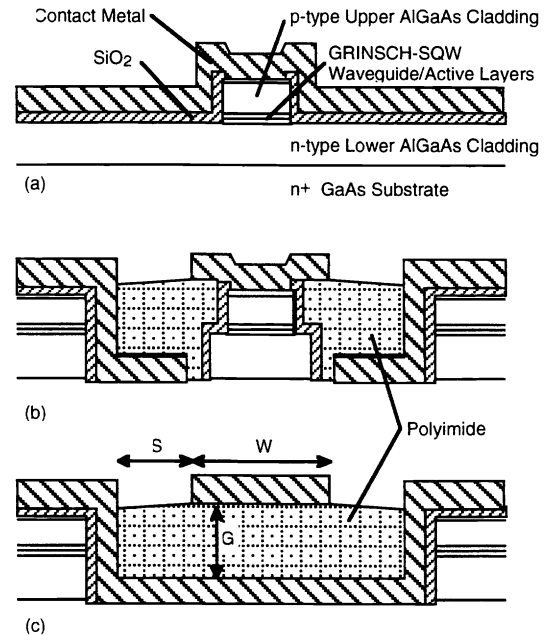


Figure 2: Cross-section views of the three principle circuit elements comprising the all-optical mm-wave signal generator. (a) Laser and amplifier active waveguide. (b) Waveguide photodiode. (c) Millimeter-wave transmission line. Key dimensions are: $W = 12 \mu\text{m}$, $S = 5 \mu\text{m}$ and $G = 10 \mu\text{m}$.

lumped photodiodes. Both 10 and 80 μm WGPD lengths were integrated with the 60 and 90 GHz lasers. All detectors are 6 μm wide, matching the width of the laser and amplifier waveguides. Calculated optical absorption within the waveguide due to the reverse-biased quantum well is 430 dB/cm. At this absorption level 10% of the light intensity will be absorbed by the photodiode in 10 μm of waveguide length and 55% in 80 μm . These values are the upper limit of WGPD efficiency. The end of the WGPD was etched at an angle⁶ to suppress reflections and feedback to the ring laser.

2.2 Fabrication

The epitaxial structure for our mm-wave generation OEIC is a single-quantum-well (10 nm) graded index separate-confinement-heterostructure in GaAs/ $\text{Al}_x\text{Ga}_{1-x}\text{As}$ with $x=0.6$ cladding layers. Overall thickness of the undoped graded layers and quantum well is 0.41 μm . Oxygen ion implantation of the p-type layers in the regions between circuit elements was used to provide electrical isolation. The implant was annealed at 850°C for 30 s to recover optical transparency while maintaining high-resistivity.^{7,8} The 6- μm wide laser, output coupler, amplifier and WGPD multilateral mode rib waveguides were formed simultaneously by chlorine reactive ion beam etching (RIBE) through the active layer. The deep trench for the WGPD and transmission line was formed in a second RIBE step. WGPD n-type ohmic contacts and transmission line ground plane metalization were deposited in the trench followed by a polyimide dielectric used to support the p-type WGPD contact and transmission line center electrode. The laser, amplifier and WGPD p-type ohmic contacts and transmission-line center electrode were deposited in a single step. Completed PICs were tested p-side up without heat sinking. Fig. 3 is an SEM image of a complete PIC. Although the straight amplifier section is broken into two separately contacted sections, all data presented here was taken by shorting the two sections together and applying a common bias current.

2.3 Results

Millimeter-wave output of PICs was measured using DC bias currents to the ring laser and amplifier. Mode-locking of the ring laser was established by reverse biasing the saturable absorber while monitoring the WGPD using Cascade co-planar probes and an HP8565E spectrum analyzer. Harmonic mixers were used at the input of the spectrum analyzer for heterodyne detection of frequencies above 50 GHz. Table 1 details the required bias conditions of the three ring diameters for stable mode-locking.

Output frequency, power and electrical linewidth of each PIC is plotted in Fig. 4. Measured output power and frequency of the 860, 430 and 290 μm diameter of rings were -12 dBm at 29.1 GHz, -23 dBm at 57.5 GHz and -27 dBm 85.2 GHz respectively. Frequency generation close to the desired value was achieved for all three laser diameters. The signals have a typical linewidth of 0.3 - 1.0 Mhz, influenced primarily by timing jitter of the pulse train. This jitter was determined by integrating the sideband noise and ranged from about 0.3 - 1.0 ns RMS, such values are not unusual for passively mode-locked semiconductor lasers.

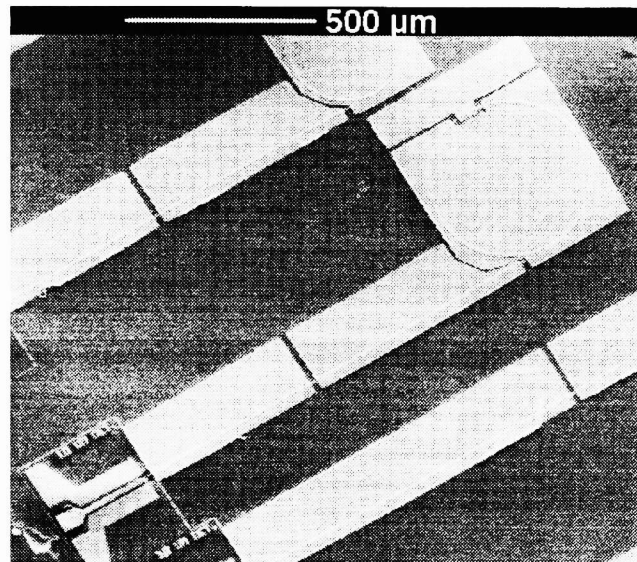


Figure 3: Electron micrograph view of complete all-optical mm-wave signal generation PIC. Total length of the circuit is less than 2 mm. Refer to Fig. 1 for itemized labeling of PIC elements.

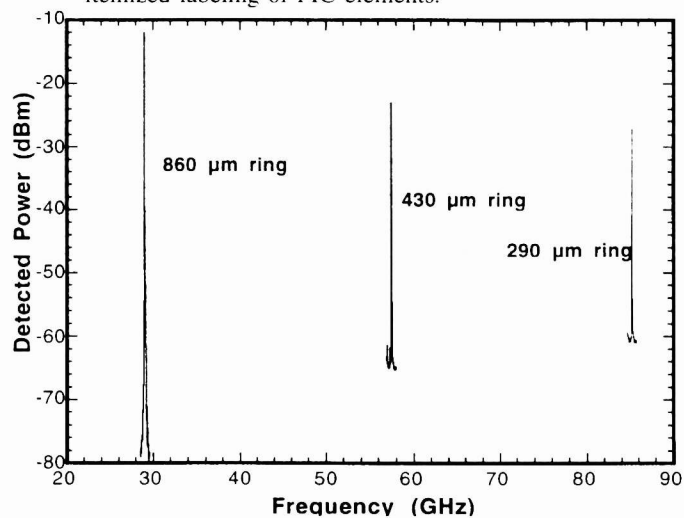


Figure 4: Measured performance of three different mm-wave signal generation PICs. Labeled ring dimensions are the diameter of ring laser used in the PIC to obtain the corresponding signal frequency.

Table 1: Operating currents and voltages for selected mm-wave generation PICs.

Ring Dia. (μm)	Ring Current (mA)	Absorber Bias (V)	Amp. Current (mA)	WGPD Bias (V)
860	130	-2.9	70	-2.9
430	180	-3.3	70	-18
290	192	-3.4	70	-17

Gain of the optical amplifier was measured in the range of 3 to 4 dB per 0.5 mm amplifier segment under CW operation. Data was taken using the same bias currents indicated in Table 1. At a fixed laser drive current, gain of an individual amplifier section is determined by the ratio of photocurrents measured using the first amplifier stage in reverse bias and then forward biasing the first amplifier stage while using the second stage in reverse bias. Since intra-band carrier relaxation times are similar to the mode-locked pulse length, measurement of CW gain is an approximation of the actual gain under mode-locked operation.

2.4 Discussion

The output frequency of our PIC is well described by (1). Cavity frequencies are approximately 5% below the predicted values, this error is dominated by variation of n_{eff} from the ideal. Output power of these first demonstration PICs is limited by WGPD efficiency. By comparison, optical autocorrelation measurements of pulse output of cleaved ring lasers have shown up to 0 dBm average power output at 87 GHz repetition rate.¹ Direct measurement of relative response of WGPDs separated from PICs shows a 20 dB roll-off at 40 GHz. WGPD performance may be limited by factors such as contact resistance, incomplete absorption within the device, and RF losses within the metal and polyimide. Considering the WGPD response of no better than -20 dB and approximately 6 dB gain available from the optical amplifier, our integrated ring lasers appear to be generating average output power similar to the earlier discrete devices.

Output power of the mm-wave PIC is influenced by a number of factors including the internal circulating power of the ring, the amount of power coupled out of the ring, gain of the amplifier and the efficiency of the photodiode. All of these require optimization to extract the maximum mm-wave power. Power extraction from the laser could be improved through use of reflective facet output couplers⁹ in place of Y-junctions, thereby improving control of the ratio of output-coupled power to circulating power. Wider pulses, up to a duty cycle of approximately 50%, could improve the output power at the fundamental frequency by as much as 10 dB. Such pulse broadening may be achievable using grating or waveguide-coupler filters within the ring cavity to reduce the lasing spectral bandwidth. Improvements in amplifier gain, detector efficiency and detector power handling capability would also increase the output power of the PIC. Use of a TWPD would increase the output by as much as a factor of 10 at these demonstration frequencies and may be required above 100 GHz due to the poor WGPD efficiency. A flared amplifier with one or more photodiodes operating in parallel at the wide amplifier output end may result in dramatic power enhancements. Finally, pulse-to-pulse timing jitter could be reduced to the femtosecond regime through the use of an electronic phase-lock loop providing feedback from the pulse output to the saturable absorber section.

3. LOW $V\pi$ MACH-ZEHNDER INTERFEROMETERS

3.1 Background

External waveguide modulators have been investigated for the past two decades to meet the evolving transmission requirements of the data communication and telecommunication fiber-optic systems. For component cost reasons, these digital systems usually use direct modulation of semiconductor lasers for short- and medium-distance links and for longer-distance links adequately supported by existing signal regenerators. However, waveguide modulators are preferred today for high-speed and long-haul communications for system cost reasons, since it allows use of wavelength-division multiplexing technologies and optical fiber amplifiers, and dramatically reduces the number of expensive signal regenerators. Specifically, as external modulation does not significantly chirp a stable carrier frequency, the dispersive effects in the fiber transmission medium permit the use of faster signaling rates and longer distances between the expensive regenerators.

The radio frequency (RF) and MW frequency photonics fields also have this requirement for bandwidth and signal fidelity as the signals of interest are analog in the 100 MHz to 20 GHz range and high-speed high-resolution analog-to-digital converters do not exist. For example, waveguide modulators are used extensively by the cable-TV industry for high-fidelity

distribution of hundreds of simultaneous signals from satellite to the home since the system distortion and noise is lower than that obtained using directly-modulated semiconductor lasers. Consequently, substantial attention by RF antenna system designers over the past five to eight years has focussed on the development of waveguide modulators that exhibit wide bandwidth (DC-20 GHz), high-sensitivity and low signal distortion ($V_{\pi} < 3$ V in a Mach-Zehnder interferometer), and low optical insertion loss (< 6 dB fiber-to-modulator-to-fiber).

3.2 Mach-Zehnder Development

Previous work at Sandia on (Al,Ga)As Mach-Zehnder interferometric modulators at $1.3 \mu\text{m}$ has focussed on reducing device optical insertion loss (6 dB fiber-to-fiber) and improving microwave bandwidth (> 20 GHz goal) in devices relying primarily on the linear electrooptic effect. We often observed relatively low extinction ratio (6-15 dB range) which was accompanied by substantial levels of polarization crosstalk in the device output. While the high extinction ratio is of second-order importance in microwave links, low extinction ratio indicates certain nonidealities we wished to understand and reduce. After eliminating splitter imbalance and sidewall scattering as significant sources of mode conversion, recent waveguide designs were developed to be highly polarization birefringent to break the degeneracy between the fundamental TE-like and TM-like eigenmodes. The current baseline waveguide design (SUID3) consists of seventy-five high index contrast layers to break the polarization degeneracy otherwise obtained.¹⁰ Using this waveguide design (Fig. 5), straight waveguides and phase modulators have been shown to retain a polarization extinction ratio in excess of 40 dB when excited by >50 dB polarization extinction ratio at the device input. We believe the detailed consideration of polarization birefringence in Sandia modulators has been the key reason we have obtained the highest extinction ratio ever reported (>40 dB) for semiconductor-based interferometers. See Figure 6 for some measured results for extinction ratio versus on-chip loss for basically three device designs. On-chip loss is measured using thermally detuned Fabry-Perot transmittance for the device biased at maximum throughput ($2\pi\text{m}$ phase matching between the two arms of the interferometer). The different waveguide

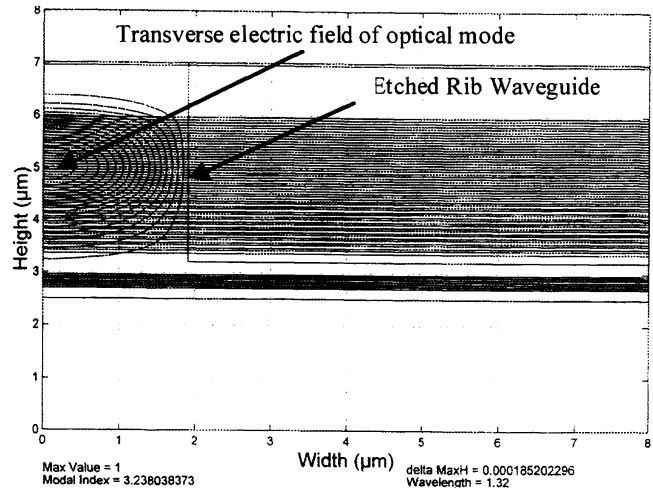


Figure 5: Calculated fundamental transverse electric field distribution for rib waveguide at $1.32 \mu\text{m}$ wavelength.

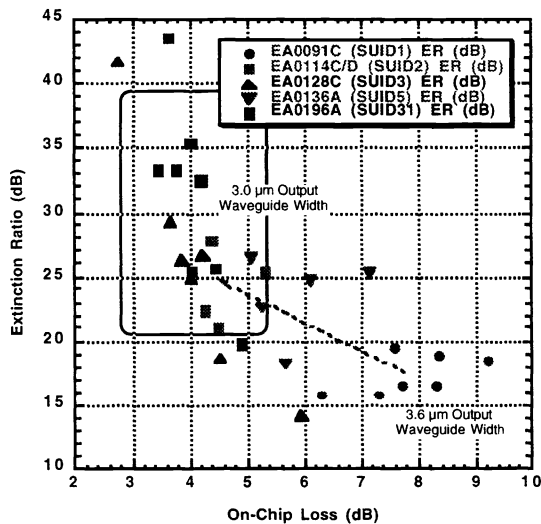


Figure 6: Extinction ratio in dB for three MZI designs. The polarization maintaining waveguides are seen to give better than 40 dB modulation.

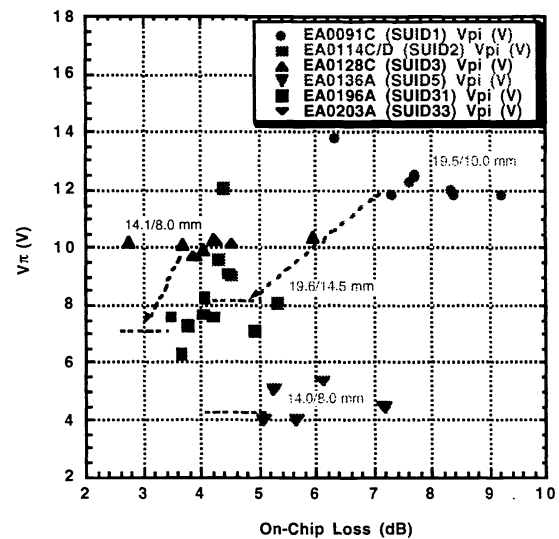


Figure 7: V_{π} for various modulator designs. Modulators with high extinction ratio (Fig. 6) are seen to clustered at 7 volts v_{π} with newer designs around 5 volts.

designs use layer doping to span the design space from low-efficiency but wide bandwidth to higher efficiency and unfortunately lower bandwidth. The calculated transverse electric attenuation coefficient for phase modulators made from these waveguide designs are about 0.07 dB/cm at 1.32 μm , including estimated losses from the Schottky contact Ti/Pt/Au metal system, assuming no chemical reactions or significant intermixing. Thermally-detuned Fabry-Perot transmission measurements on these simple devices give about 0.25 dB/cm which we believe is dominated by the scattering from the etched sidewalls defining the rib boundary or other effects not adequately modeled. Previous work on similar waveguide designs suggest that the electrooptic efficiency of the baseline design is about 56 V-mm at 1.32 μm . Figure 7 shows modulator sensitivity results for the extinction ratio results of Figure 6. In Figure 7, the modulator and electrode lengths are listed next to the plotted data. Increasing the electrode length to 45mm for the baseline design will

increase the modulator sensitivity (reduce the $V\pi$) to an anticipated $V\pi = 1.24$ V. Effects of this scaleup are predicted in Figure 8 for several waveguide designs. Efforts were undertaken to scaleup current processes from 3in quadrants to full 3in-wafers to allow these long electrical-optical interaction lengths.

Measured results for extinction ratio and sensitivity are shown in Figures 9 and 10, respectively. The extinction ratio and the on-chip loss were both degraded from predictions based on simply scaling the results from shorter structures. We believe the decreased extinction ratio was caused by nonuniformities in processing these devices over large areas wherein the probability of the waveguide intersecting a material or processing defect is significantly higher than in shorter devices. The increased loss over the predicted values may be related to the degraded extinction ratio for the same reasons. We believe the measured sensitivity is due to problems associated with nonuniform contact along the device length. Design and process modifications are underway to remedy these process problems. The goal is to realize a < 1V-sensitive, >20 GHz-bandwidth, <6 dB-loss Mach-Zehnder interferometer.

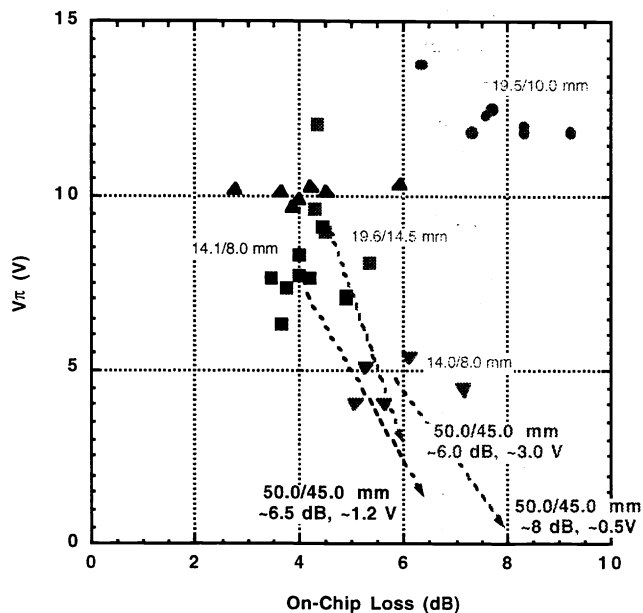


Figure 8: Effects of scale-up, increasing length so as to reduce $V\pi$, on the devices of Fig. 7. Arrows show calculated trends of $V\pi$ and on-chip loss.

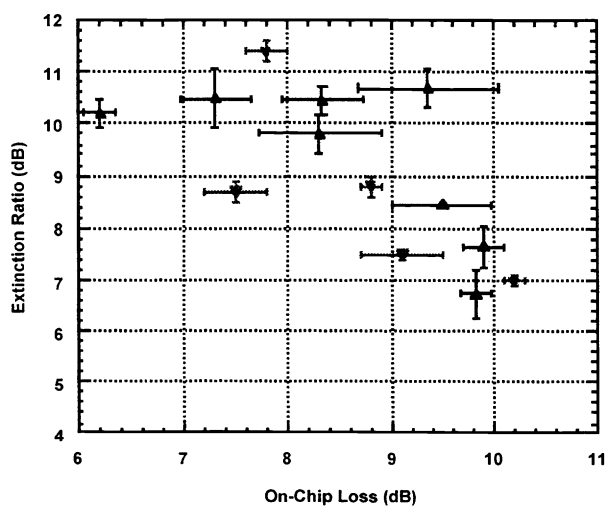


Figure 9: Extinction ratio for scale-up (lengthened) MZIs.

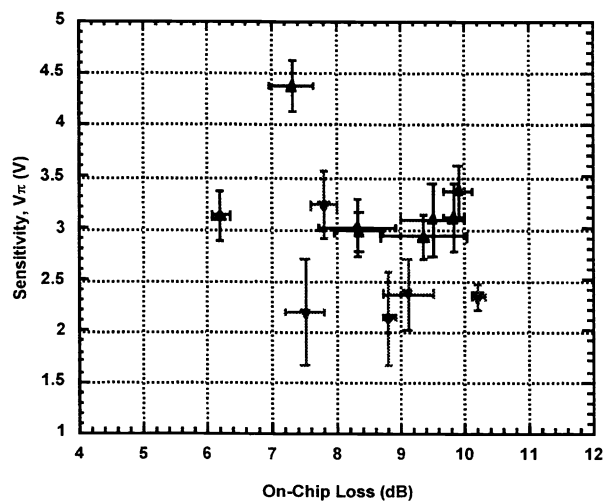


Figure 10: $V\pi$ of scaled-up (lengthened) MZIs. Modulation voltages as low as 2.2 volts are observed.

4. CONCLUSION

In summary, we have demonstrated the first PIC for direct generation of mm-wave frequencies. This PIC integrates a passively mode-locked semiconductor ring laser with an optical amplifier and high-speed waveguide photodiode. By generating and amplifying a train of optical pulses and using an integrated waveguide photodiode to convert the optical pulses into an electrical signal, this circuit has been used to generate -23 and -27 dBm of mm-wave power at 57.5 and 85.2 GHz respectively. Similarly, direct sampling of the saturable absorber has generated -12 dBm at 29.1 GHz. PICs using this concept can be used in a wide variety of applications where a very compact, lightweight mm-wave source is required.

Polarization-maintaining MZIs in AlGaAs have been demonstrated with extinction ratios better than 40 dB and on-chip loss below 6 dB. Reduction of V_p to 2.2 V has been achieved through the use of longer modulators. This reduction came at the cost of reduced extinction ratio caused by increased cumulative light scattering effects in the longer devices. We expect that improvements in waveguide quality will dramatically improve the extinction ratio. All aspects of this MZI design and performance-to-date support the goal of a < 1V-sensitive, >20 GHz-bandwidth, <6 dB-loss Mach-Zehnder interferometer fabricated in AlGaAs.

ACKNOWLEDGMENTS

This work was supported by United States Department of Energy under Contract DE-AC04-94AL85000. Sandia is a multiprogram laboratory operated by Sandia Corporation, a Lockheed-Martin Company, for the United States Department of Energy.

REFERENCES

- 1 G. A. Vawter, A. Mar, V. Hietala, J. Zolper and J. Hohimer, "All Optical Millimeter-Wave Electrical Signal Generation Using an Integrated Mode-Locked Semiconductor Ring Laser and Photodiode", *IEEE Phot. Technol. Lett.* **9**(12), 1634-1636 (1997).
- 2 J. P. Hohimer and G. A. Vawter, "Passive mode locking of monolithic semiconductor ring lasers at 86 GHz", *Appl. Phys. Lett.* **63**(12), 1598-1600 (1993).
- 3 V. M. Hietala, G. A. Vawter, T. M. Brennan and B. E. Hammons, "Traveling-wave photodetectors for high-power large-bandwidth applications", *IEEE Trans. on Microwave Th. and Tech.* **43**(9), 2291-2297 (1995).
- 4 K. S. Giboney, R. L. Nagarajan, T. E. Reynolds, S. T. Allen, R. P. Mirin, M. J. Rodwell and J. E. Bowers, "Travelling-wave photodetectors with 172-GHz bandwidth and 76 GHz bandwidth-efficiency product", *IEEE Phot. Technol. Lett.* **7**(4), 412-414 (1995).
- 5 L. Y. Lin, M. C. Wu, T. Itoh, T. A. Vang, R. E. Muller, D. L. Sivco and A. Y. Cho, "Velocity-Matched Distributed Photodetectors with High-Saturation power and large bandwidth", *IEEE Phot. Technol. Lett.* **8**(10), 1376-1378 (1996).
- 6 J. P. Hohimer, G. A. Vawter, D. C. Craft and G. R. Hadley, "Improving the Performance of Ring Diode Lasers by Controlled Reflection Feedback", *Appl. Phys. Lett.* **61**(9), 1013-1015 (1992).
- 7 J. C. Zolper, A. G. Baca and S. A. Chalmers, "Thermally Stable Oxygen Implant Isolation of p-type AlGaAs", *Appl. Phys. Lett.* **62**(20), 2536-2538 (1993).
- 8 R. P. Bryan, J. J. Coleman, L. M. Miller, M. E. Givens, R. S. Averback and J. L. Klatt, "Impurity induced disordered quantum well heterostructure stripe geometry lasers by MeV oxygen implantation", *Appl. Phys. Lett.* **55**(2), 94-96 (1989).
- 9 J. P. Hohimer, G. R. Hadley and G. A. Vawter, "Semiconductor Ring Lasers With Reflection Output Couplers", *Appl. Phys. Lett.* **63**(3), 278-280 (1993).
- 10 C. T. Sullivan, G. A. Vawter and et. al., "Packaging of (Al,Ga)As Photonic Integrated Circuits", *IEEE MTT-S, International Microwave Symposium: Workshop on Microwave and Millimeter Wave Optoelectronic Integrated Circuit Modules*, Denver, CO (1997).